Journal of Environmental Chemical Engineering 10 (2022) 107058

Contents lists available at ScienceDirect

Journal of Environmental Chemical Engineering

journal homepage: www.elsevier.com/locate/jece

Development of novel electrochemical sensor based on PtNPs-SeNPs-FTO nanocomposites via electrochemical deposition for detection of hydrogen peroxide

Nilesh S. Dumore, Mausumi Mukhopadhyay *

Department of Chemical Engineering, Sardar Vallabhbhai National Institute of Technology, Surat 395007, Gujarat, India

ARTICLE INFO

Editor: Dr. G. Palmisano

Keywords:
FTO
Electrochemical sensor
Hydrogen peroxide
Platinum nanoparticles
Selenium nanoparticles
Electrodeposition
Cyclic voltammetry and Amperometry

ABSTRACT

The PtNPs-SeNPs-FTO nanocomposites as electrochemical sensor was developed via electrochemical deposition method for hydrogen peroxide detection. The synthesis and growth of selenium nanoparticles (SeNPs), platinum nanoparticles (PtNPs) and nanocomposites of PtNPs-SeNPs on fluorine doped tin oxide (FTO) substrate by using electrochemical deposition for H_2O_2 detection was reported. Morphological and structural study of bare FTO, PtNPs-FTO, SeNPs-FTO and PtNPs-SeNPs-FTO sensor was confirmed by FEGSEM, EDS mapping, and XPS. Morphology of synthesized PtNPs and SeNPs decorated on the FTO surface showed nano-flower structure and spherical in shape respectively. The XPS analysis was carried out to identify elemental composition on the surface-modified PtNPs-SeNPs-FTO sensor. The survey spectra of PtNPs-SeNPs-FTO electrode displayed a considerable strong peak of C, F, Sn, O, Pt, and Se, which confirmed the existence of these elements on the FTO surface. The synthesized SeNPs-FTO, PtNPs-FTO, and PtNPs-SeNPs-FTO sensor displayed wide range of linear concentration response from 0.01 to 40 mM and response time 0.5 s. The synthesized SeNPs-FTO, PtNPs-FTO and PtNPs-SeNPs-FTO sensor showed sensitivity of 0.4 μA mM^{-1} cm^{-2} (R^2 =0.9904), 17.2 μA mM^{-1} cm^{-2} (R^2 =0.9917) and 7.3 μA mM^{-1} cm^{-2} (R^2 = 0.9835) respectively. The SeNPs-FTO, PtNPs-FTO and PtNPs-SeNPs-FTO based sensor also demonstrated high selectivity towards detection of H_2O_2 with interfering agents.

1. Introduction

Electrochemical detection of hydrogen peroxide (H_2O_2) detection plays an important role in various fields, including food processing, environmental analysis, clinical diagnostic, pharmaceutical, and biomedical devices [1–3]. The development of a sensitive, accurate, selective, reliable, and economical sensor for H_2O_2 detection is necessary in this era. The level (100 μM or more) of H_2O_2 keep intracellular thermogenesis (warming of human cells), which is most essential to human life. It also works as an insulin that helps to maintain the sugar in the human body [4,5]. Some variation found in H_2O_2 level may cause diseases like osteoporosis, asthma, damage to the lysosomal membrane, diabetic vasculopathy, atherosclerosis, cancer, and some neurodegenerative diseases [3,4,6]. Maintaining a normal level of H_2O_2 is essential for normal cell functions, and intracellular signaling transduction and its higher-level concentration are affected to be extremely hazardous [7–9]. Thus, the precise H_2O_2 detection is very essential for the biological and environmental analyses. Many detection techniques are available for the detection of H_2O_2, such as chromatography [10], spectrometry [11], chemiluminescence [12], fluorescence [13], and electrochemical method [14]. Among all, the detection of H_2O_2 by the electrochemical method mostly preferable due to its high sensitivity, fast response, low cost, simple, good selectivity, and easy to operate as compared to the other traditional methods.

Nowadays, noble metal such as platinum (Pt) based nanocomposites have raised great research interests due to the self-supported structure and some unique properties. Platinum nanoparticles (PtNPs) show excellent electroanalytical investigation properties towards hydrogen peroxide and have been widely used in electrochemical sensors with high sensitivity and rapid amperometric response to detect the different target of analytes such as ethanol, methanol, glucose, and hydrogen peroxide [15–19]. However, pure PtNPs catalyst is relatively expensive and can be easily poisoned by adsorbed intermediates. Various literature have been reported that PtNPs modified with other noble metal [20], metal alloy [17], metal oxide [19], carbon nanostructure [21] and semiconductor material [1] exhibit enhanced catalytic activity of H_2O_2

* Corresponding author.
E-mail address: mmu@ched.svnit.ac.in (M. Mukhopadhyay).

https://doi.org/10.1016/j.jece.2021.107058
Received 22 September 2021; Received in revised form 15 December 2021; Accepted 21 December 2021
Available online 24 December 2021

detection and the tolerance to poisoning. Researchers show more and more attention towards semiconductor and metal structure nanocomposites due to their various applications in electronic, sensor, catalysis and optoelectronic device [22,23]. Selenium (Se) has various important properties and use such as semiconductor, catalytic activity, sensing, free radical scavenging and high photoconductivity [24,25]. Nanocomposites reinforced with platinum nanoparticles (PtNPs) and selenium nanoparticles (SeNPs) have shown improvement in electrodeposited Pt and Se coating stability while providing cost-effective alternative to pure Platinum (Pt) electrochemical sensor. Depending on the composition, the PtNPs and SeNPs nanocomposite exhibit enhanced catalytic activity and electro-conductivity to Selenium nanoparticles electrochemical sensor due to synergic effect.

A few literature have reported the construction of Pt nanoparticles with Se nanomaterial as the non-enzymatic H_2O_2 sensor by drop-casting methods [1,26]. It shows linear detection range from 0.01 to 15 mM hydrogen peroxide (H_2O_2) concentration and detection limit 0.0031 mM [1]. Microbial SeNPs-ITO sensor fabricated by drop-casting methods show linear detection range from 0.005 to 0.6 mM hydrogen peroxide (H_2O_2) concentration, detection limit 0.003 mM and sensitivity 16.54 $\mu A\ mM^{-1}\ cm^{-2}$ ($R^2 = 0.9904$) [27]. The synthesis of SeNPs/HRP/GCE sensor by using drop casting method, show linear detection range from 0.0017 to 0.53 mM hydrogen peroxide (H_2O_2) concentration and detection limit 0.009 mM [28]. According to previous work, selenium nanoparticles (SeNPs) - fluorine-doped tin oxide (FTO) sensor prepared by using spin coating method, show linear detection range from 0.1 to 20 mM hydrogen peroxide (H_2O_2) concentration and sensitivity 104.2 $\mu A\ mM^{-1}\ cm^{-2}$ ($R^2 = 0.9904$). Transparent conducting oxide (TCO) like fluorine-doped tin oxide (FTO) have been preferably used for electrodeposition techniques in various area such as electrochromic mirrors, sensors, solar cells, advanced bioanalytical device and solar energy conversion due to its properties like transparency, thermal stability, fully biocompatible, nontoxic and economical high conductivity [29]. The electrochemical techniques like linear sweep voltammetry (LSV), cyclic voltammetry (CV), chronoamperometry and sono-electrodeposition show more preference towards the electrodeposition of nanostructures on the TCO surface [30]. In this technique, various parameters of experiment like precursor salt concentration, applied potential, current density and time of deposition can be used to control the size, morphology, nucleation and growth rate of the nanostructures [31]. The electrodeposition technique is a very fast, clean, does not required any chemical reducing agent required less energy, less consumption of raw material, and no unwanted by-product formation [32]. Additionally, multi-layers of mono or multi metals nanostructure can be easily formed by electrodeposition technique [33]. The fabrication of Pt and Se based nanocomposites on the surface of FTO for the detection of H_2O_2 via electrodeposition technique has not been reported yet.

In this present work, the preparation of PtNPs-SeNPs-FTO sensor via electrochemical deposition is reported. The CV and amperometric response of SeNPs-FTO, PtNPs-FTO, and PtNPs-SeNPs-FTO is also reported. The amperometric interference study of SeNPs-FTO, PtNPs-FTO, and PtNPs-SeNPs-FTO with interference agent like ascorbic acid (AA), urea (UR), sucrose (SU), glucose (GU), and sodium chloride (SC) are also carried out and shows the response for the detection of hydrogen peroxide is reported. The prepared PtNPs-FTO, SeNPs-FTO, and PtNPs-SeNPs-FTO are characterized by FEGSEM, EDS mapping, and XPS.

2. Material and methods

2.1. Materials

Sodium selenite and sucrose were obtained from Himedia Laboratories Pvt. Ltd. Mumbai, India. Chloroplatinic acid hexahydrate, glucose, and commercial fluorine-doped tin oxide coated glass (FTO glass) were purchased from Sigma-Aldrich, USA. Ascorbic acid was purchased from Rankem, India. Sodium hydroxide, hydrochloric acid, hydrogen peroxide, sodium chloride, sodium citrate, urea, and acetone were obtained from Finer, India. Deionized water was prepared in the laboratory via Millipore Elix setup (India) and used for cleaning and experiment. 0.1 M Phosphate buffer solution (PBS) (at neutral pH) was prepared by mixing Na_2HPO_4 and NaH_2PO_4 as standard stock solutions.

2.2. Methods

2.2.1. Preparation of SeNPs-FTO sensor via electrodeposition method

An aqueous solution of sodium selenite and sodium citrate was prepared in DI water (Indian Patent Application Number – 202121031002). The pH of aqueous solution was maintained with the help of HCl (0.1 N) and NaOH (0.1 N). This aqueous solution of sodium selenite and sodium citrate was used for the electrodeposition process. For each precleaned FTO substrate, linear sweep voltammetry (LSV) was used to form a SeNPs film on FTO with the three-electrode system of PGSTAT Autolab system in the dispersion of sodium selenite and sodium citrate as supporting electrolyte. The scan range of LSV was 0 to − 1.5 V with 10, 20, 40, 50, and 100 mV/s scan rate at temperature 28 ± 2 °C for LSV cycles 1, 2, 3, 4, and 5. Prepared SeNPs-FTO sensor was kept for annealing process in the tubular furnace and then dried overnight into the oven to get SeNPs-FTO sensor.

2.2.2. Preparation of PtNPs-FTO sensor via electrodeposition method

An aqueous solution of chloroplatinic acid hexahydrate was prepared in phosphate buffer solution (PBS) at a neutral pH electrolyte. Then, the pH of aqueous solution was maintained with the help of HCl (0.1 N) and NaOH (0.1 N), which was further used for the electrodeposition process (Indian Patent Application Number - 202121031002). For each precleaned FTO substrate, the LSV was used to form PtNPs film on the FTO surface with the three-electrode system of the PGSTAT Autolab system. The scan range of LSV was 0 to − 0.5 V at 10, 20, 40, 50, and 100 mV/s scan rate up to cycles 4, then chronoamperometry was used at applied potential − 0.4 V for the period of 50, 100, 200, 300, 400, and 500 s. Prepared PtNPs-FTO sensor kept for annealing process in the tubular furnace and then dried overnight into the oven to get PtNPs-FTO sensor.

2.2.3. Preparation of SeNPs- PtNPs-FTO sensor via electrodeposition method

Initially, the optimized condition of the PtNPs-FTO sensor (performed LSV was 0 to − 0.5 V at 10, 20, 40, 50 and 100 mV/s scan rate up to cycles 4, then chronoamperometry used at applied potential − 0.4 V for the period of 50, 100, 200, 300, 400, and 500 s) was used for the preparation of the first PtNPs film on the surface of FTO for SeNPs-PtNPs-FTO sensor. Afterwards, the suitable condition of SeNPs-FTO was used for the preparation of the SeNPs film on PtNPs-FTO film for SeNPs-PtNPs-FTO sensor. Prepared SeNPs-PtNPs-FTO sensor kept for annealing process in the tubular furnace and then dried overnight into the oven to get SeNPs- PtNPs-FTO sensor.

2.2.4. Preparation of PtNPs-SeNPs-FTO sensor via electrodeposition method

Initially, the optimized condition of the SeNPs-FTO sensor (performed 3 LSV cycles, scan range 0 to − 1.5 V with 10, 20, 40, 50 and 100 mV/s scan rate at room temperature) was used for the preparation of the first SeNPs film on the surface of FTO for PtNPs-SeNPs-FTO sensor. Afterwards, the suitable condition of PtNPs-FTO was used for the preparation of the PtNPs film on SeNPs-FTO film for PtNPs-SeNPs-FTO sensor. Prepared PtNPs-SeNPs-FTO sensor kept for annealing process in the tubular furnace and then dried overnight into the oven to get PtNPs-SeNPs-FTO sensor (Indian Patent Application Number – 202121031002).

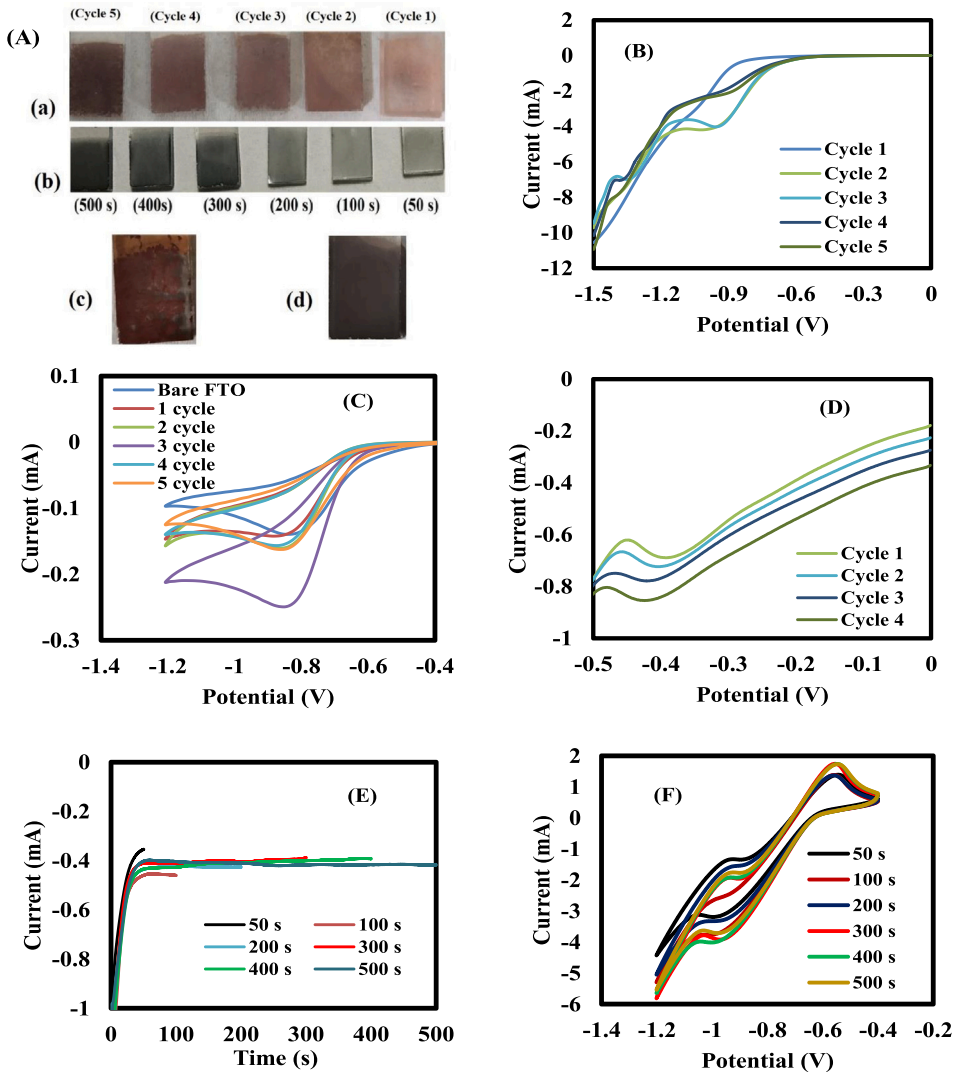

Fig. 1. (A) Image of SeNPs-FTO (a), PtNPs-FTO (b), SeNPs-PtNPs-FTO (c) and PtNPs-SeNPs-FTO (d) after electrochemical deposition. (B) LSV of the SeNPs-FTO electrode for cycles 1, 2, 3, 4, and 5. (C) CVs performance of SeNPs-FTO electrode after LSV cycles 1, 2, 3, 4, and 5. (D) LSV of PtNPs-FTO electrode for cycles 1, 2, 3, and 4. (E) CA of PtNPs on FTO electrode for the time period of 50, 100, 200, 300, 400 and 500 s (F) CVs performance of PtNPs-FTO after CA period of time for 50, 100, 200, 300, 400 and 500 s.

2.3. Characterization

The surface and cross-section morphology of SeNPs-FTO, PtNPs-FTO, and PtNPs-SeNP-FTO were investigated by field emission gun scanning electron microscope with energy dispersive spectroscopy (FEGSEM and EDS) on a JSM 7600F (JEOL Co., Japan). X-ray Photoelectron Spectroscopy (XPS) of PtNPs-SeNPs-FTO was used to investigate the surface chemistry of materials with Oxford instruments Germany. XPS analysis of PtNPs-SeNPs-FTO was done to identify elemental composition of synthesized PtNPs and SeNPs nanocomposite on the FTO surface through electrodeposition method.

2.4. Electrochemical measurements

All electrochemical experiments were performed via Autolab (PGSTAT 204) electrochemical workstation with NOVA 2.1.4 software. In the electrochemical experiments, a three-electrode system consists of a modified (with SeNPs, PtNPs, and PtNPs-SeNPs-FTO) and unmodified FTO were used as working electrode with Pt-mesh (with area 2 cm^2) and saturated calomel electrode (SCE) as the counter and a reference electrode, respectively. Electrochemical H_2O_2 sensing was performed in a 0.1 M PBS (at neutral pH) as the electrolyte. The potential scan was ranged from − 0.4 to − 1.2 V at 50 mV/s.

3. Results and discussions

3.1. Synthesis and optimization of the electrochemical deposition process of SeNPs-FTO, PtNPs-FTO, SeNPs-PtNPs-FTO and PtNPs-SeNPs-FTO

The synthesis and growth of selenium nanoparticles (SeNPs), platinum nanoparticles (PtNPs), and nanocomposites of SeNPs and PtNPs on the surface of FTO substrate by using electrochemical deposition technique was as shown in Fig. 1(A). In the electrochemical deposition, the SeNPs start deposited on the FTO substrate when it forms red film on the FTO surface, as shown in Fig. 1(A) (a). The PtNPs start deposited on FTO substrate forming a black film on the surface of FTO electrode, as shown in Fig. 1(A) (b). The growth and formation of SeNPs and PtNPs on the FTO surface through electrochemical deposition, was as shown in Fig. 1 (A) (c). The growth and formation of PtNPs and SeNPs on the FTO surface through electrochemical deposition, was as shown in Fig. 1(A) (d).

The LSV was performed for the synthesis of SeNPs film on the FTO surface via electrochemical deposition at temperature 28 ± 2 °C for cycles 1, 2, 3, 4, and 5 from 0 to − 1.5 V with scan rate (50 mV/s) as shown in Fig. 1 (B). The LSV of cycle 3 showed a strong reduction peak for SeNPs on the FTO surface. During LSV scan from 0 to − 1.5 V two reduction peaks at $C_1 = -0.92$ V and $C_2 = -1.3$ V was observed. These two reduction peaks represent a nucleation process of four-electron

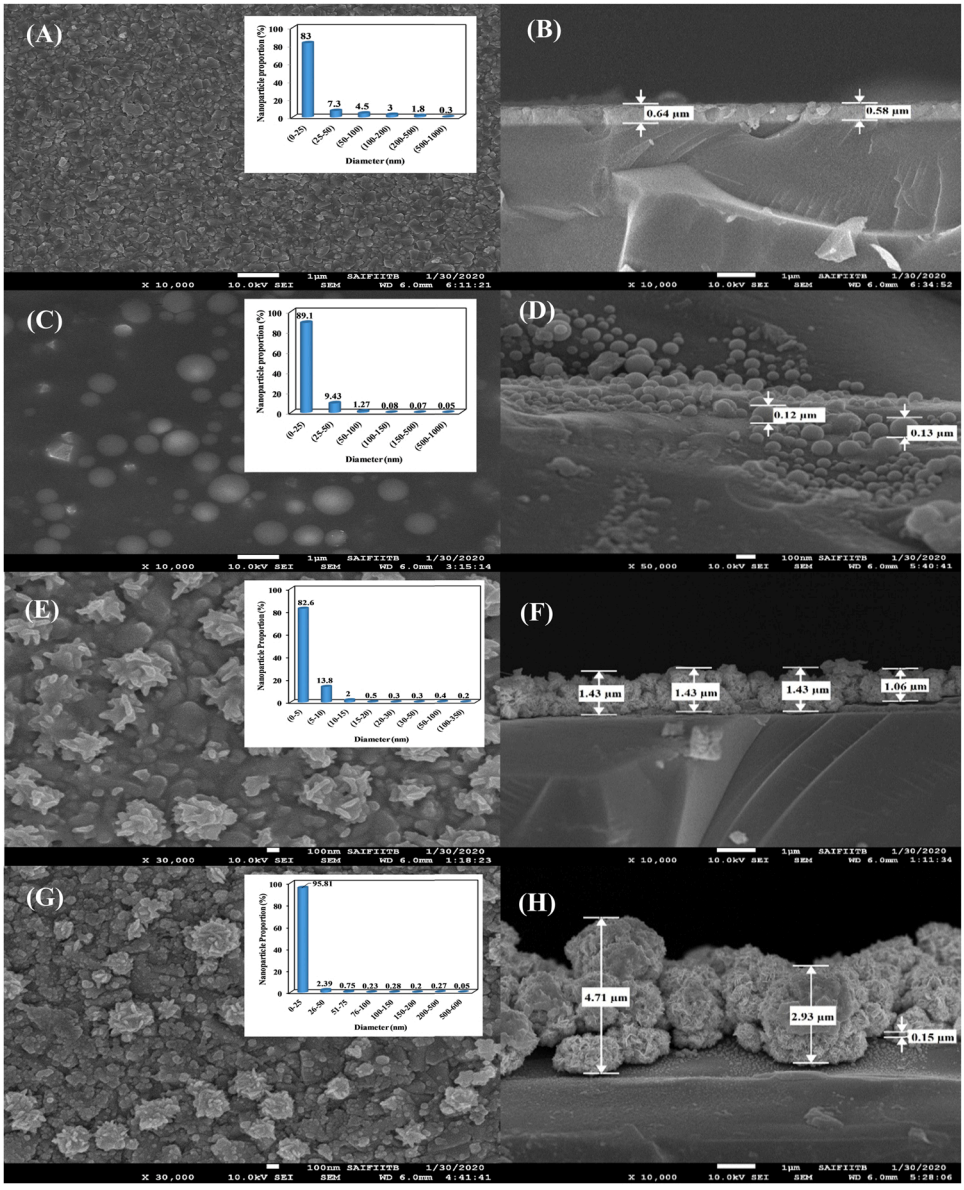

Fig. 2. FEGSEM image (A) Top-view surface (Inset represents percentage wise size distribution of SnO_2) and (B) Cross-sectional of FTO, (C) Top-view surface (Inset represents percentage wise size distribution of SeNPs-FTO) and (D) cross-sectional of SeNPs-FTO, (E) Top-view surface (Inset represents percentage wise distribution of PtNPs-FTO) and (F) cross-sectional of PtNPs-FTO, (G) Top-view surface (Inset represents percentage wise size distribution of PtNPs-SeNPs-FTO) and (H) cross-sectional of PtNPs-SeNPs-FTO.

reduction from Se^{4+} to Se^0. Cyclic voltammetry (CV) was performed for synthesized SeNPs-FTO electrodes for different LSV cycles 1, 2, 3, 4, and 5 at temperature 28 ± 2 °C in 0.1 M PBS (at neutral pH) electrolyte with at least 1 mM H_2O_2 at 50 mV/s scan rate as shown in Fig. 1(C). The reduction peak of SeNPs-FTO was observed at the potential of − 0.8 to − 0.9 V in 0.1 M PBS (at neutral pH). All SeNPs-FTO electrodes obtained after LSV 1, 2, 3, 4, and 5 cycles from electrochemical deposition showed a reduction of H_2O_2 approximately at − 0.85 V. The optimized condition considered for growth and synthesis of SeNPs on the FTO surface through electrochemical deposition via LSV after 3 cycles because CV of synthesized SeNPs-FTO electrode showed the highest electrocatalytic performance towards the H_2O_2 reduction in Fig. 1(C). The LSV performance of electrochemical deposition of PtNPs film on the FTO surface was at temperature 28 ± 2 °C for cycles 1, 2, 3, and 4, as shown in Fig. 1 (D). The LSV showed that the intensity of the reduction peak increases with an increasing number of LSV cycles at − 0.4 V. The LSV of cycle 4 showed a strong reduction peak for the electro-deposition process of platinum on the FTO surface. The LSV of the cathodic part for a solution was traced on the FTO electrode with 50 mV/s scan rate. During LSV scan from 0 to − 0.5 V reduction peaks at $C_1 = -0.4$ V was observed. That reduction peaks represent a nucleation process of the electron reduction from chloroplatinic acid to PtNPs during LSV study. The reduction peak at − 0.4 V was continuously increase from -0.68 to − 0.84 V with increasing LSV cycle from 1 to 4. The stable growth of PtNPs on FTO substrate was identified by chronoamperometry (CA). The chronoamperometry was used to electrochemical deposition of PtNPs on FTO substrate for the time period of 50, 100, 200, 300, 400, and 500 s at applied potential − 0.4 V, as shown in Fig. 1 (E). The CVs of synthesized PtNPs-FTO was performed in 0.1 M PBS electrolyte with 1 mM H_2O_2 between − 0.4 V and − 1.2 V at scan rate 50 mV/s at 50, 100, 200, 300, 400, and 500 s. The result was shown as shown in Fig. 1 (F).

The oxidation and reduction peak of PtNPs-FTO were observed between the potential of − 0.5 to − 0.6 V and − 0.9 to − 1.0 V in 0.1 M PBS (at neutral pH) electrolyte. The PtNPs-FTO electrodes showed the reduction of H_2O_2 approximately at − 0.95 V. The optimized condition considered for the synthesis and growth of PtNPs on the FTO surface by electrochemical deposition via CA was at applied potential − 0.4 V for 400 s, as synthesized PtNPs-FTO electrode showed the highest electrocatalytic performance towards the H_2O_2 reduction at this condition. PtNPs-SeNPs-FTO and SeNPs-PtNPs-FTO sensor was prepared with the help of optimized condition of SeNPs-FTO and PtNPs-FTO sensor by electrodeposition method.

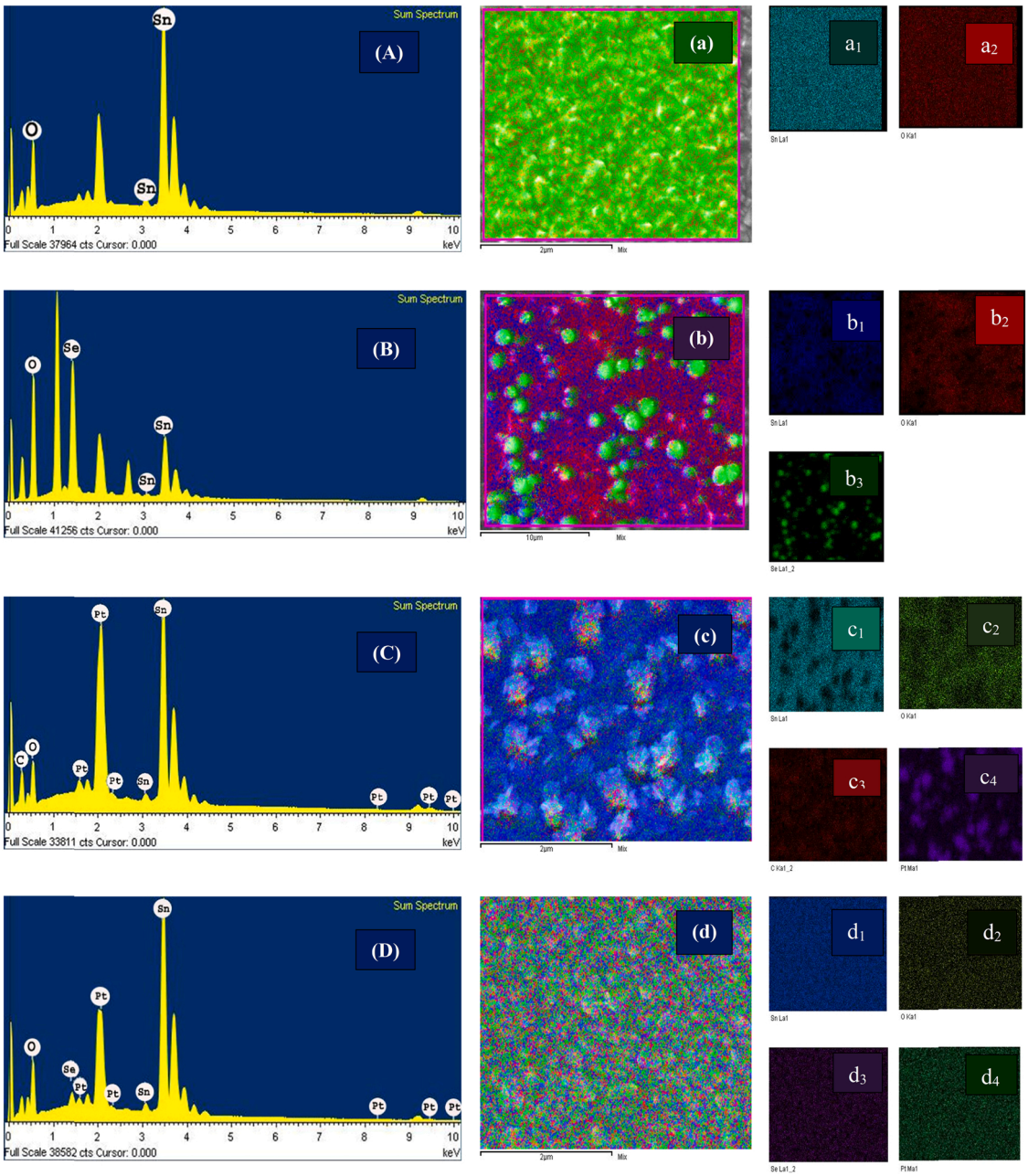

Fig. 3. (A) EDS spectra of FTO electrode [(a) EDS Mapping of FTO, and a_1 and a_2 show the elemental mapping of Sn, and O.], (B) EDS spectra of SeNPs-FTO electrode [(b) EDS Mapping of SeNPs-FTO and b_1, b_2, and b_3 show the elemental mapping of Sn, O, and Se], (C) EDS spectra of PtNPs-FTO electrode [(c) EDS Mapping of PtNPs-FTO and c_1, c_2, c_3, and c_4 show the elemental mapping of Sn, O, C and Pt], (D) EDS spectra of PtNPs-SeNPs-FTO electrode [(d) EDS Mapping of PtNPs-SeNPs-FTO and d_1, d_2, d_3 and d_4 show the elemental mapping of Sn, O, Se and Pt].

3.2. Morphology and structural analysis of bare FTO, PtNPs-FTO, SeNPs-FTO and PtNPs-SeNPs-FTO

Morphology, size, and structural characterization of bare FTO, SeNPs-FTO, PtNPs-FTO, and PtNPs-SeNPs-FTO was studied using field gun emission scanning electron microscopy (FEGSEM) in FTO, as shown in Fig. 2(A) top-view surface [inset represents percentage wise size distribution of tin oxide (SnO_2)] and (B) cross-sectional of FTO, (C) top-view surface (inset represents percentage wise size distribution of SeNPs-FTO) and (D) cross-sectional of SeNPs-FTO, (E) top-view surface (inset represents percentage wise size distribution of PtNPs-FTO) and (F) cross-sectional of PtNPs-FTO, (G) top-view surface (inset represents percentage wise size distribution of PtNPs-SeNPs-FTO) and (H) cross-sectional of PtNPs-SeNPs-FTO.

The top-view surface of Fig. 2(A) displayed bare FTO glass reveals an uneven and random distribution of tin oxide grains with an obvious grain boundary and irregular shape, and large size. The bare FTO coatings showed faceted grains with sizes ranging from 10 to 927 nm (with 95% particles having a size less than equal to 100 nm). The thickness of tin oxide film on the glass substrate was 0.6 ± 0.05 μm from the cross-sectional view of FTO as in Fig. 2(B). The synthesized SeNPs decorated on the FTO surface were uniform and spherical in shape. The particles size of SeNPs on the FTO surface was in the ranges from 10 to 981 nm (with 89% particles having a size less than equal to 25 nm) from the top-view surface of SeNPs-FTO in Fig. 2(C). The FEGSEM analysis identified the synthesis and growth of SeNPs on the FTO surface via the electrochemical deposition method. The thickness of SeNPs on the FTO glass substrate was 0.13 ± 0.05 μm from the cross-sectional view of

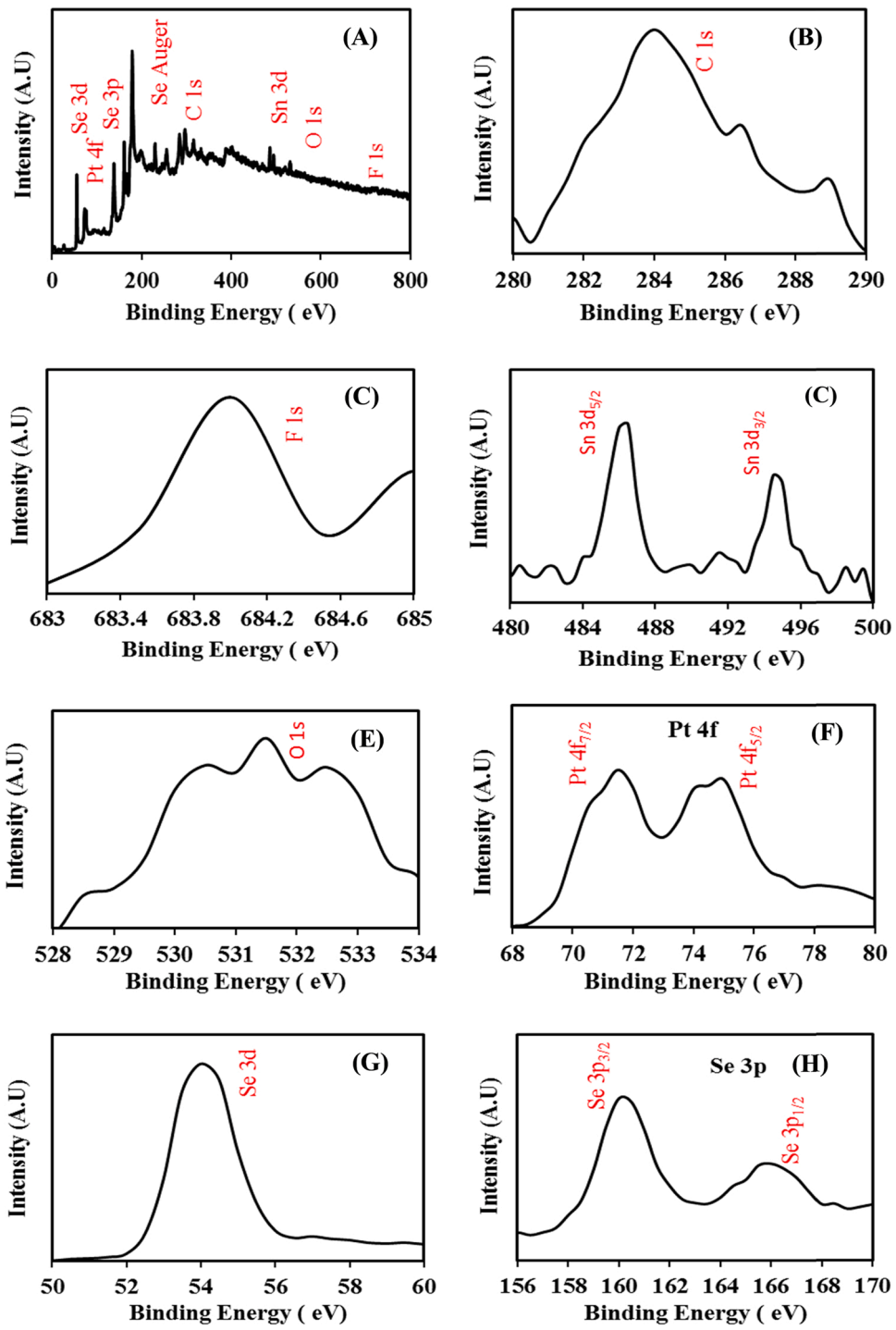

Fig. 4. XPS spectra of the synthesized PtNPs-SeNPs-FTO sensor (A) survey spectrum, (B) C 1s, (C) F 1s, (D) Sn 3d, (E) O 1s, (F) Pt 4f, (G) Se 3d, and (H) Se 3p.

SeNPs-FTO in Fig. 2(D).

The morphology of synthesized PtNPs decorated on the FTO surface was well organized (flower with many petals like) structure from top-view of the surface of PtNPs-FTO in Fig. 2(E). The size of PtNPs on the FTO surface was ranging from 3 to 343 nm (with 83% particles having a size less than equal to 5 nm). The FEGSEM analysis confirmed the synthesis and growth of PtNPs on the FTO surface via the electrochemical deposition method. The thickness of PtNPs on the FTO glass substrate was 1 ± 0.5 μm from the cross-sectional view of PtNPs-FTO in Fig. 2(F).

Initially, SeNPs coated on the surface of FTO then PtNPs coated on the surface of SeNPs-FTO via electrodeposition method. The FEGSEM analysis of PtNPs-SeNPs-FTO nanocomposite (Fig. 2G and H) showed the morphology and particles size of the PtNPs and SeNPs on the FTO surface. The size of PtNPs-SeNPs nanocomposite on the FTO surface was ranging from 3 to 614 nm (with 96% particles having a size less than equal to 25 nm) from top-view of the surface of PtNPs-FTO in Fig. 2(G). The FEGSEM analysis showed that synthesized and growth of PtNPs and SeNPs were properly dispersed and identical in shape (PtNPs-flower with many petals and SeNPs-spherical). The cross-sectional view of PtNPs-SeNPs-FTO (Fig. 2H) suggest that thickness of PtNPs and SeNPs on the surface of FTO was 4 ± 1.5 μm and 0.1 ± 0.05 μm respectively. Fig. 2(H) illustrated growth and thickness of PtNPs on the surface of

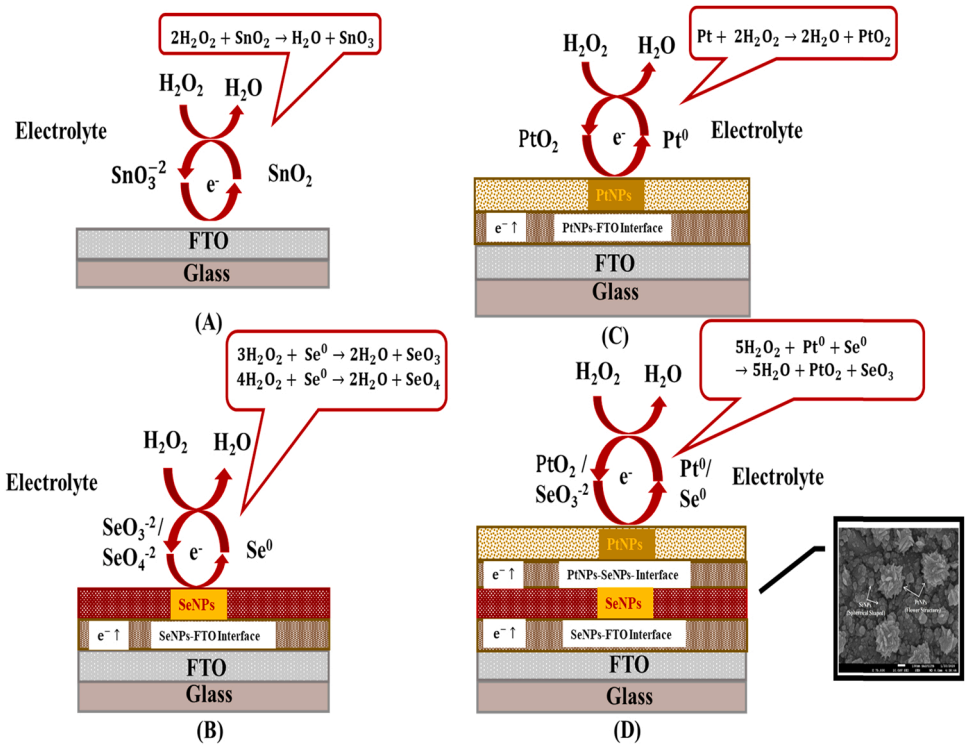

Fig. 5. Proposed mechanism of H_2O_2 detection on the surface of (A) bare FTO, (B) SeNPs-FTO, (C) PtNPs-FTO, and (D) PtNPs-SeNPs-FTO, electrode in 0.1 M PBS (at neutral pH) electrolyte.

SeNPs-FTO was increases as compared to FTO surface (Fig. 2(F)). Fig. 2 (E) and (G) exhibited that the number of PtNPs (Flower structure) on the surface of SeNPs-FTO obtained less compared to bare FTO surface, this is why PtNPs-FTO sensor showed that better performance towards H_2O_2 detection as compared to PtNPs-SeNPs-FTO sensor. From study of FEGSEM image (Fig. 2E–H) observed that SeNPs responsible for controlling growth and synthesis of PtNPs on the SeNPs-FTO surface. The particle size distribution (percentage-wise) of bare FTO, SeNPs-FTO, PtNPs-FTO, and PtNPs-SeNPs-FTO according to FEGSEM image was represented in Fig. 2(A), (C), (E) and (G).

3.3. EDS mapping analysis of bare FTO, PtNPs-FTO, SeNPs-FTO and PtNPs-SeNPs-FTO

EDS mapping of bare FTO, PtNPs-FTO, SeNPs-FTO, and PtNPs-SeNPs-FTO, was shown in Fig. 3. The EDS spectra of bare FTO showed the elemental analysis peak signal for Tin (Sn) and oxygen (O), as shown in Fig. 3(A). The purity of FTO was confirmed that no other peak corresponding to any impurity found in the EDS spectra.

EDS mapping of FTO shown in Fig. 3(a) overlay of Tin (Sn) and Oxygen (O) elements. Fig. 3(a_1) and (a_2) showed the separate homogenous mapping of Sn element (Bluish-green) and O element (Red), respectively. EDS mapping of bare FTO exhibits the uniform distribution of Sn and O elements on the glass substrate. The EDS spectra of SeNPs-FTO was observed elemental peaks signal for Selenium (Se), Tin (Sn), and Oxygen (O) as shown in Fig. 3(B). The purity of SeNPs on the FTO surface was confirmed that no other peak corresponding to any impurity found in the EDS spectra. EDS Mapping of SeNPs-FTO shown in Fig. 3(b) Overlay of Selenium (Se), Tin (Sn), and Oxygen (O) elements. Fig. 3(b_1) (b_2), and (b_3) showed separate homogenous mapping of Sn element (Blue), O element (Red), and Se element (Green), respectively. EDS mapping of SeNPs-FTO exhibit the uniform distribution of Se, Sn, and O elements on the glass substrate. The EDS spectra of PtNPs-FTO were observed elemental peaks signals for Platinum (Pt), Tin (Sn), and Oxygen (O) as shown in Fig. 3(C). The purity of PtNPs on the FTO surface was confirmed that no other peak corresponding to any impurity found in the EDS spectra. The peak of the carbon element was also obtained due to carbon-coated on PtNPs-FTO before analysis for sample preparation of FEG-SEM and EDS mapping. EDS Mapping of PtNPs-FTO shown in Fig. 3(c) showed an overlay of Platinum (Pt), Carbon (C), Tin (Sn), and Oxygen (O) elements. Fig. 3(c_1)–(c_4) showed separate homogenous mapping of Sn element (Bluish-green), O element (Green), C element (Red), Pt element (violet), respectively. EDS mapping of PtNPs-FTO exhibit the uniform distribution of Pt, Sn, and O elements on the glass substrate. The EDS spectrum of PtNPs-SeNPs-FTO was observed elemental peak signal for Platinum (Pt), Selenium (Se), Tin (Sn), and Oxygen (O) shown in Fig. 3(D). The purity of PtNPs and SeNPs on the FTO surface was confirmed that no other peak corresponding to any impurity showed in the EDS spectra. EDS mapping of PtNPs-SeNPs-FTO shown in Fig. 3(d) Overlay of Platinum (Pt), Selenium (Se), Tin (Sn), and Oxygen (O) elements. Fig. 3(d_1) (d_2), (d_3), and (d_4) showed the separate homogenous mapping of Sn element (Blue), O element (yellow), Se element (violet), and Pt element (Green). EDS mapping of PtNPs-SeNPs-FTO exhibited the uniform distribution of Pt, Se, Sn, and O elements on the glass substrate.

3.4. X-ray photoelectron spectroscopy (XPS) analysis of PtNPs-SeNPs-FTO

XPS analysis was carried out to identify the elemental composition on the surface-modified PtNPs-SeNPs-FTO sensor, and the results obtained of XPS analysis were shown in Fig. 4. The wide range spectrum of XPS analysis for synthesized PtNPs-SeNPs-FTO sensor via electrochemical deposition methods was shown in Fig. 4(A). The survey spectra of PtNPs-SeNPs-FTO electrode display a considerable strong peak of C, F, Sn, O, Pt, and Se, which confirmed the existence of these elements on the surface of FTO. Fig. 4(B) showed high resolution of C 1s XPS spectra, the peaks signal at 284.0, 286.5, and 288.9 eV corresponding to C–C, C–O, and O–C═O, respectively. Fig. 4(C) showed a high-resolution of F 1s XPS spectra with only one strong peak signal which represented to F–Sn

bond. Fig. 4(D) showed a high-resolution of Sn 3d XPS spectra. It showed two peaks signal corresponding to Sn $3d_{5/2}$ and Sn $3d_{3/2}$. The peak signal was fitted into two peaks at 486.9 eV and 487.4 eV, which were assigned to Sn–O and Sn–F, respectively. Fig. 4(E) showed a high-resolution of O 1s XPS spectra displays two fitted peaks signal located at 531.1 and 532.2 eV, which assigned to Sn–O, and C–O [34]. Fig. 4(F) showed Pt 4f spectrum of PtNPs-SeNPs-FTO showed two strong peaks around at 71.1 and 74.5 eV, which represent to the metallic platinum. The possible chemical valence states showing doublet in Pt XPS spectrum due to spin-orbit split of Pt $4f_{7/2}$ and $4f_{5/2}$ metallic Pt^0 doublet around at 71.1 eV and 74.5 eV. The material characterization indicated that PtNPs were successfully decorated onto the FTO surface [35]. Fig. 4(G) and (H) showed the high-resolution of Se 3d and Se 3p ($3p_{3/2}$ and $3p_{1/2}$) XPS spectra. Meanwhile, the binding energy peak of Se 3d located around at 54.5 eV, along with Se $3p_{3/2}$ and Se $3p_{1/2}$ at 160.0 and 166.0 eV, all indicate the − 2 oxidation chemical state of Se. Signals were also examined in the spectra of Se 3d at the binding energy around 56.5 eV due to the deposition of a bit of metalloid Se on the FTO surface through the electrochemical deposition method [36].

3.5. Mechanism of H_2O_2 detection

The proposed mechanism for electro-reduction of H_2O_2 on the bare FTO, SeNPs-FTO, PtNPs-FTO, and PtNPs-SeNPs-FTO surface includes the following steps

$$H_2O_2 + e^- \xrightarrow{r.d.s.} OH_{(a.s.)} + OH^- \quad \ldots \quad (1)$$

$$OH_{(a.s.)} + e^- \rightarrow OH^- \quad \ldots \quad (2)$$

$$2OH^- + 2H^+ \rightarrow 2H_2O \ldots \quad (3)$$

In previous work [37], Eqs. (1)–(3) and possible reaction mechanism of H_2O_2 electro-reduction were the same as mentioned in the deposition methods of selenium nanostructure on the surface of FTO was used spin coating methods.

The proposed mechanism of H_2O_2 detection on the bare FTO, SeNPs-FTO, PtNPs-FTO and PtNPs-SeNPs-FTO sensor in the 0.1 M PBS (at neutral pH) revealed in the Fig. 5(A)–(D).

Case I. Fig. 5(A) demonstrated the reaction mechanism of bare FTO with H_2O_2 in the 0.1 M PBS (at neutral pH) electrolyte.

$$H_2O_2 + SnO_2 \rightarrow H_2O + SnO_3 \ldots \quad (4)$$

Case. II: Fig. 5(B) demonstrated the proposed mechanism of SeNPs-FTO in the 0.1 M PBS (at neutral pH) electrolyte with H_2O_2 was the same with previous work. The deposition of SeNPs on the surface of the FTO electrode.

$$3H_2O_2 + Se^0 \rightarrow 2H_2O + SeO_3 \quad \ldots \quad (5)$$

$$4H_2O_2 + Se^0 \rightarrow 3H_2O + SeO_4 \ldots \quad (6)$$

Case. III: Fig. 5(C) demonstrated the proposed mechanism of PtNPs-FTO in the 0.1 M PBS (at neutral pH) electrolyte with H_2O_2. The electro-reduction of H_2O_2 on the modified surface of PtNPs-FTO electrode is mediated by the conversion of platinum into platinum oxide in PBS (at neutral pH) electrolyte is observed, which works as an electron transfer system, and H_2O_2 reduced to H_2O [38].

$$2H_2O_2 + Pt^0 \rightarrow 2H_2O + PtO_2 \ldots \quad (7)$$

Case IV. : Fig. 5(D) demonstrated the proposed mechanism of PtNPs-SeNPs-FTO in the 0.1 M PBS (at neutral pH) electrolyte with H_2O_2. The electro-reduction of H_2O_2 on the modified surface of the PtNPs-SeNPs-FTO electrode in the 0.1 M PBS (at neutral pH) electrolyte is observed. The PtNPs-SeNPs-FTO electrode is electrochemically formed into platinum oxide and selenite, which works as an electron transfer system, and H_2O_2 is reduced to H_2O [37].

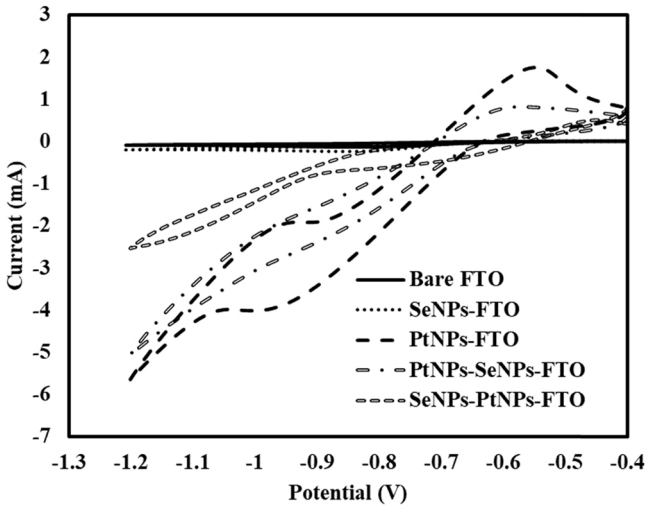

Fig. 6. CV of Bare FTO, SeNPs-FTO, PtNPs-FTO, and PtNPs-SeNPs-FTO electrode in 0.1 M PBS (at neutral pH) electrolyte with 1 mM H_2O_2.

$$5H_2O_2 + Pt^0 + Se^0 \rightarrow 5H_2O + PtO_2 + SeO_3 \ldots \quad (8)$$

3.6. Electrochemical response of SeNPs-FTO, PtNPs-FTO, SeNPs-PtNPs-FTO and PtNPs- SeNPs-FTO

The electrochemical response of bare FTO electrode, SeNPs-FTO, PtNPs-FTO, SeNPs-PtNPs-FTO, and PtNPs-SeNPs-FTO towards H_2O_2 reducing was carried out in 0.1 M PBS (at neutral pH) electrolyte with 1 mM H_2O_2 in the potential range between − 0.4 V and − 1.2 V with scan rate 50 mV/s as shown in Fig. 6. The CVs curve of bare FTO electrode, SeNPs-FTO, PtNPs-FTO, SeNPs-PtNPs-FTO and PtNPs-SeNPs-FTO exhibited a cathodic peak near − 0.85 V, − 0.85 V, − 0.95 V, − 0.95 V, and − 0.95 V, which was the representation of electrochemical reduction of H_2O_2. The potential value of the SeNPs-FTO electrode for H_2O_2 sensing was found − 0.85 V, nearly the same in both spinning coating and electrochemical deposition method [37]. The reduction of H_2O_2 increases intensity in peak current as a function of H_2O_2 concentration, indicating the potential of the bare FTO, SeNPs-FTO, PtNPs-FTO, SeNPs-PtNPs-FTO, and PtNPs-SeNPs-FTO electrode to be applied in an amperometric detection of H_2O_2. The cathodic reduction current peak of bare FTO, SeNPs-FTO, PtNPs-FTO, SeNPs-PtNPs-FTO, and PtNPs-SeNPs-FTO electrode was − 0.096, − 0.212, − 5.564, − 2.546, and − 5.068 mA. The reduction peak current was observed in the negative scan of CV, which was attributed to the reduction of H_2O_2. PtNPs-FTO electrode showed highest cathodic reduction current peak of 1 mM H_2O_2 into PBS (at neutral pH) electrolyte solution than SeNPs-FTO, SeNPs-PtNPs-FTO, and PtNPs-SeNPs-FTO electrode. The PtNPs-FTO electrode showed good electrocatalytic activity towards H_2O_2 due to good conductivity and high surface area of PtNPs (flower structure with many petals) morphology in the case of PtNPs-FTO electrode.

The number of PtNPs (flower structure) on the surface of SeNPs-FTO showed less compared to FTO surface according to FEG-SEM analysis that is why PtNPs-FTO sensor showed that good electrocatalytic behavior towards H_2O_2 detection as compared to PtNPs-SeNPs-FTO sensor. The bare FTO exhibited negligible electrochemical response of

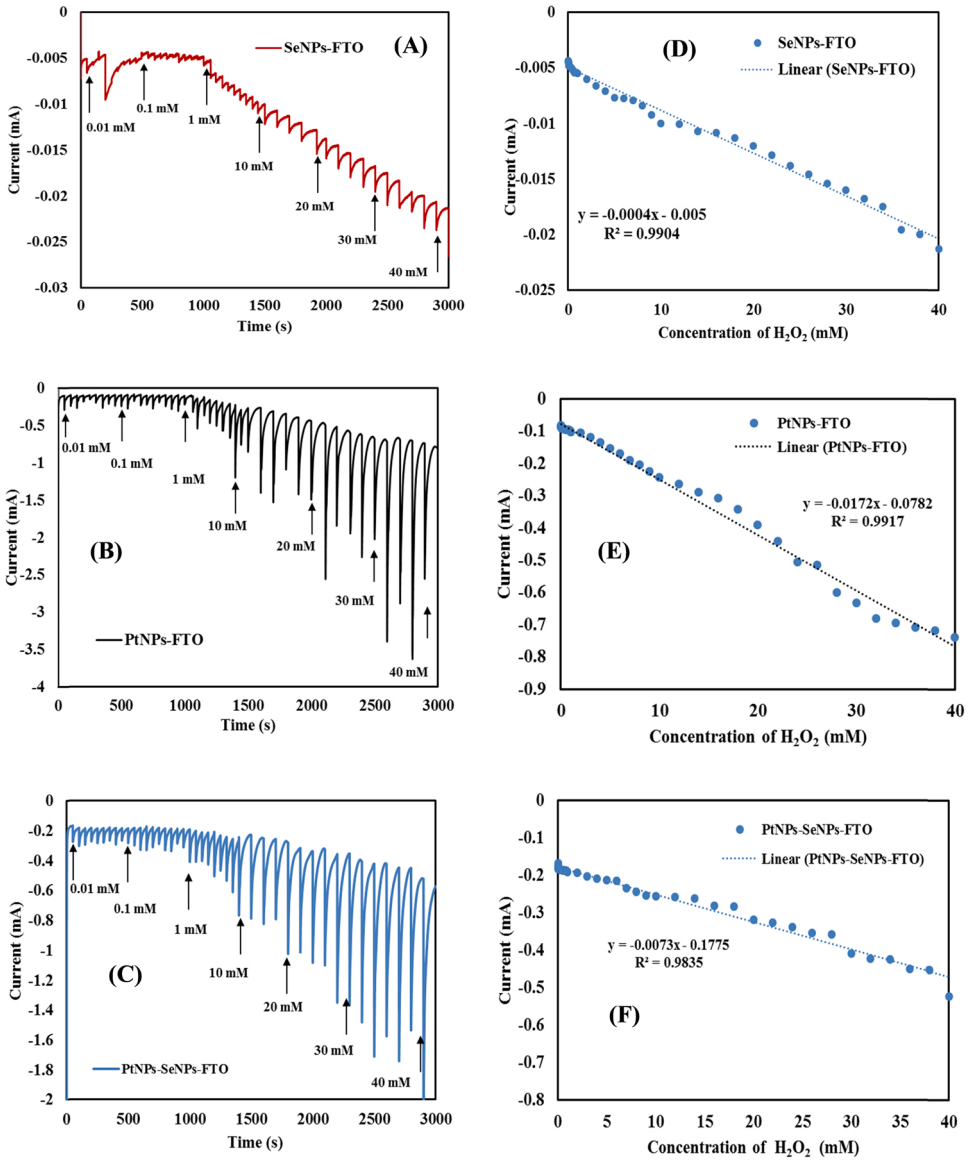

Fig. 7. Amperometric i-t curve after successive addition of H_2O_2 for (A) SeNPs-FTO at applied potential − 0.85 V vs SCE, (B) PtNPs-FTO at Applied potential − 0.95 V vs SCE, (C) PtNPs-SeNPs-FTO at applied potential − 0.95 V vs SCE. Calibration plot of H_2O_2 sensing (Current vs. Concentration) for (D) SeNPs-FTO, (E) PtNPs-FTO (F) PtNPs-SeNPs-FTO.

1 mM H_2O_2 into PBS (at neutral pH) electrolyte solution compare to SeNPs-FTO, PtNPs-FTO, PtNPs-SeNPs-FTO and PtNPs-SeNPs-FTO. CV results suggested that PtNPs-SeNPs-FTO electrode performance for H_2O_2 reduction better than the SeNPs-PtNPs-FTO electrode because SeNPs diminish conductivity of PtNPs in case of SeNPs-PtNPs-FTO. Further process carried out with SeNPs-FTO, PtNPs-FTO and PtNPs-SeNPs-FTO electrode for amperometric detection of H_2O_2.

3.7. Amperometric study of SeNPs-FTO, PtNPs-FTO, and PtNPs- SeNPs-FTO

The amperometric study of SeNPs-FTO, PtNPs-FTO, PtNPs-SeNPs-FTO sensor on the basis of electrocatalytic reduction towards detection of H_2O_2 was carried out as shown in Fig. 7(A)–(C). The characteristic response of the amperometric i-t curve of SeNPs-FTO, PtNPs-FTO, and PtNPs-SeNPs-FTO after the successive addition of H_2O_2 in 0.1 M PBS (at neutral pH) at an applied potential of − 0.85, − 0.95, and − 0.95 V versus SCE, respectively. SeNPs-FTO, PtNPs-FTO, and PtNPs-SeNPs-FTO sensor showed instant variation of H_2O_2 concentration at applied potential of − 0.85, − 0.95, and − 0.95 V respectively. SeNPs-FTO, PtNPs-FTO, and PtNPs-SeNPs-FTO sensor were exhibited a corresponding linear plot for detection of the H_2O_2 as shown in Fig. 7(D)–(F). The SeNPs-FTO, PtNPs-FTO, PtNPs-SeNPs-FTO sensor showed wide linear detection from 0.01 to 40 mM H_2O_2 concentration and the response time of 0.5 s. The limit of detection for PtNPs-SeNPs-FTO was 0.005 mM. The synthesized SeNPs-FTO, PtNPs-FTO and PtNPs-SeNPs-FTO sensor showed sensitivity of 0.4 μA mM^{-1} cm^{-2} (R^2 =0.9904), 17.2 μA mM^{-1} cm^{-2} (R^2 =0.9917), and 7.3 μA mM^{-1} cm^{-2} (R^2 =0.9835) respectively. According to previous work, the SeNPs-FTO sensor showed a linear detection range from 0.1 to 20 mM H_2O_2 concentration and sensitivity of 104.2 μA mM^{-1} cm^{-2} (R^2 = 0.9904). But present SeNPs-FTO sensor shows a wide linear detection range and less sensitivity compared to the previously reported SeNPs-FTO sensor. This was due to the different morphology of SeNPs nanoparticles (nanorods) in previous work [37]. The morphology, dimensions, surface area, grain, and pore size have primarily affected electrochemical sensing parameters. The peculiar nanostructures such as porous nanotubes and nanofibers enhance the inner and outer surface area, improve porosity, and

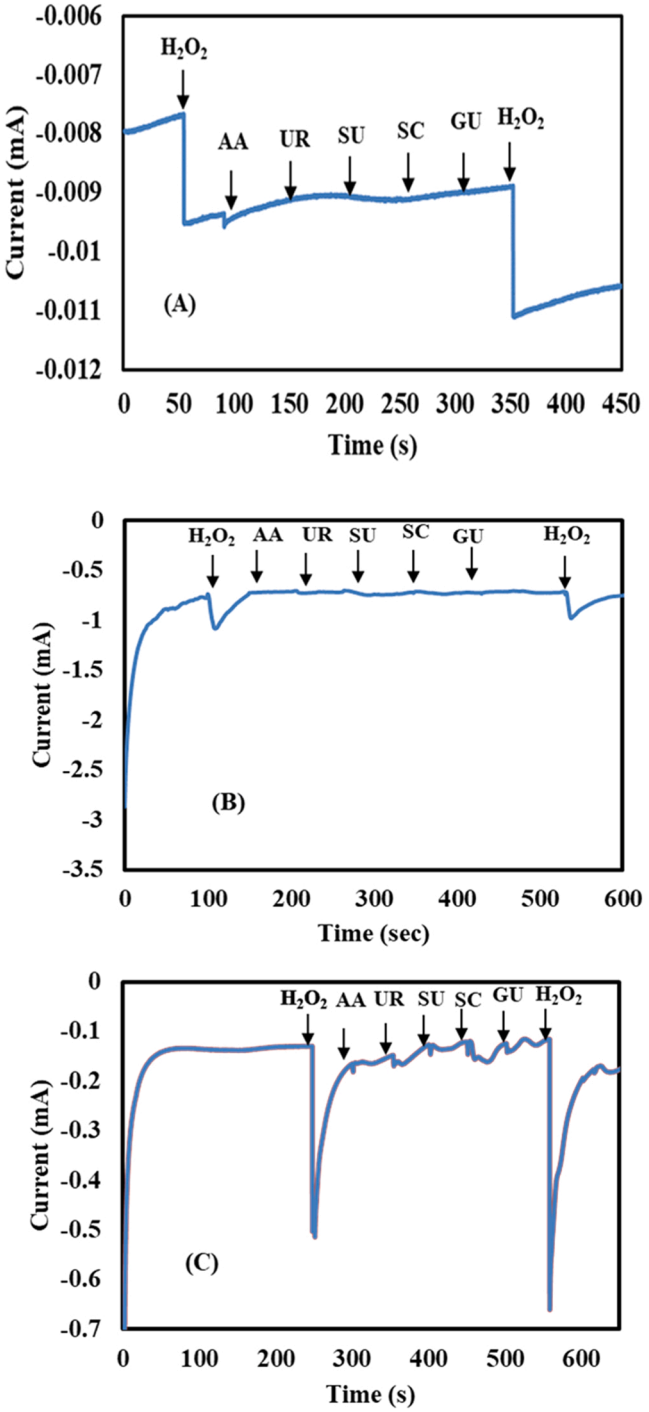

Fig. 8. Interference study of (A) SeNPs-FTO, (B) PtNPs-FTO, and (C) PtNPs-SeNPs-FTO for addition of H_2O_2 (0.5 mM) and interference agent (each 0.5 mM) like AA, UR, SU, SC and GU.

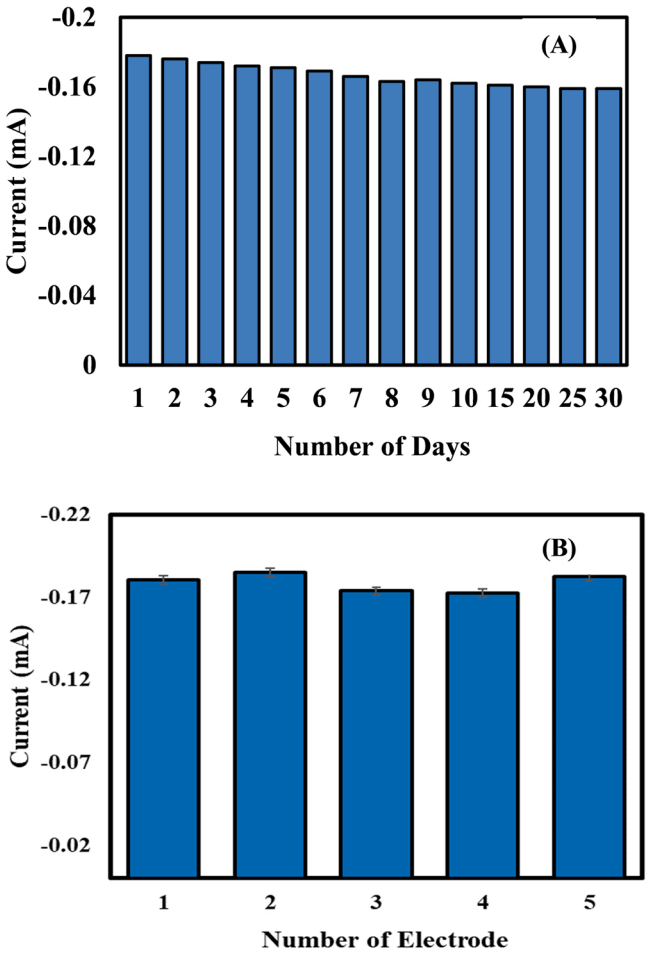

Fig. 9. (A) Stability of modified PtNPs-SeNPs-FTO sensor for H_2O_2 detection and investigated for addition of 1 mM H_2O_2 over one month at applied potential − 0.95 V (vs. SCE), (B) Reproducibility of PtNPs-SeNPs-FTO sensor performed in 1 mM H_2O_2 in PBS (at neutral pH) electrolyte.

excellent flexibility, improve mass and electron transfer between electrode and electrolyte, and maximize the number of active sites. These properties have potentially improved the linear ranges, sensitivity, and selectivity [39]. In previous work, synthesized selenium nanoparticles (nanorods shape) were deposited on the surface of FTO by spin coating methods. The selenium nanoparticles coating on the FTO surface using spin coating method is high as compared to the electrodeposition method of selenium nanoparticles [37].

In previous work [37], SeNPs-FTO (nanorods) show high sensitivity as compare to SeNPs-FTO (nano-spheres) in the present work. Nanoscale wire and nanotube have the capability of high detection sensitivity and very high surface area [40]. When the concentration of H_2O_2 is high, a huge amount of reduction products was formed on the surface of the modified electrode, which prevented the adsorbing and reduction of H_2O_2, and thus, the sensitivity was decreased [4]. Although, the obtained experimental result of PtNPs-SeNPs-FTO and PtNPs-FTO electrochemical sensor showed good performance for detecting H_2O_2 with high sensitivity at higher H_2O_2 concentration (40 mM). Also, studied the stability and reproducibility of the developed PtNPs-SeNPs-FTO and PtNPs-FTO based sensor, but PtNPs-SeNPs-FTO nanocomposites sensor have economical as compared to PtNPs-FTO sensor.

3.8. *Interference study of SeNPs-FTO, PtNPs-FTO and PtNPs-SeNPs-FTO*

The interference study of the SeNPs-FTO, PtNPs-FTO, and PtNPs-SeNPs-FTO sensor was investigated using the interfering agent like AA, UR, SU, SC and GU on the detection of H_2O_2, as shown in Fig. 8(A)–(C). For this study of SeNPs-FTO, PtNPs-FTO and PtNPs-SeNPs-FTO sensor, interfering agents at least 0.5 mM each like AA, UR, SU, SC and GU were added along with successive addition of as low as 0.5 mM H_2O_2 into 0.1 M PBS (at neutral pH). While the change in the current response after the successive addition of the interfering agent was not indicated any obvious response compared to H_2O_2. The examination results showed that the potential of SeNPs-FTO, PtNPs-FTO, and PtNPs-SeNPs-FTO electrodes for the H_2O_2 detection through electrochemical sensing and confirmed that PtNPs-SeNPs-FTO displayed a high

Table 1
Comparison of electrochemical H_2O_2 sensing performance with various nanocomposite electrode.

Nanocomposite	Method used of film	Shape of nanoparticles	Linear detection range (mM)	Sensitivity (μA mM^{-1} cm^{-2})	Reference
PtNPs-SeNPs-FTO PtNPs-FTO SeNPs-FTO	Electrodeposition	Pt-Nanoflower Se-Nanosphere	0.01–40	7.3 17.2 0.4	This work
SeNPs-FTO	Spin coating methods	Se-Nanotube	0.1–20	104.2	[37]
Se/ Pt Nanocomposite	Drop casting method	Se-Nanowire Pt- Nanotube	0.001–15	3.1	[1]
Microbial SeNPs	Drop casting method	Se-Spherical	.0.005–0.6	16.54	[27]
SeNPs using Bacillus Subtilis	Drop casting method	Se-Spherical	–	0.08	[41]
Pt-Au-rGO-GCE	Electrodeposition	–	0.001–1.68	–	[42]
CuO-FTO	Spin coating methods	CuO-Nanorods	0.25–18.75	84.89	[14]
Pt-SnO_2@C	Drop casting method	Sphere-like	0.001–0.17	241.1	[19]
RGO-PtNPs-GCE	Physical adsorption and Electrodeposition method	–	0.0005–3.475	0.459	[43]
Pt-Au/G-CNTs	Drop casting method	–	0.002–8.561	313.4	[44]

selectivity to H_2O_2 detection in the existence of common interference agent.

The long-term stability of modified PtNPs-SeNPs-FTO electrodes for H_2O_2 sensing was also investigated by amperometric measurement over the period of one month, as shown in Fig. 9(A). The amperometric current response reduced up to 10% of its initial value for 1 mM H_2O_2 after one month stored at room temperature. To check the reproducibility, five sets of the PtNPs-SeNPs-FTO sensor were performed under the same condition 1 mM H_2O_2 in PBS (at neutral pH) electrolyte as shown in Fig. 9(B). The response of current for five sets of PtNPs-SeNPs-FTO sensor showed -0.18063 ± 0.005, -0.18509 ± 0.005, -0.1738 ± 0.005, -0.17249 ± 0.005 and-0.18231 ± 0.005 mA, respectively. This showed that the PtNPs-SeNPs-FTO sensor was shown reproducibility and stability.

Comparative performance results of H_2O_2 sensing response (linear detection range and sensitivity) using numerous nanocomposites based electrodes with this current work for the detection of hydrogen peroxide were provided in Table 1. The synthesized SeNPs-FTO, PtNPs-FTO, and PtNPs-SeNPs-FTO electrochemical sensor found good sensing response towards analytes with a wide detection range compared to previous work from literature results. The prepared SeNPs-FTO, PtNPs-FTO, and PtNPs-SeNPs-FTO non-enzymatic electrochemical sensors were highly sensitive and wide linear detection range towards the H_2O_2 sensing related to various sensors represented in the literature.

In the amperometric study, the PtNPs-SeNPs-FTO sensor exhibited variance in behavior of amperometric current after the consecutive addition of H_2O_2 and formation of Pt to PtO_2 and Se to ions of SeO_3 due to the occurrence of PtNPs and SeNPs on the FTO surface assists to fast transfer electron through the interface of PtNPs-SeNPs-FTO. Therefore, the development of PtNPs-SeNPs-FTO exhibited an essential source for H_2O_2 sensing and high catalytic activity to reduce H_2O_2.

4. Conclusions

In conclusion, SeNPs-FTO, PtNPs-FTO, and PtNPs-SeNPs-FTO sensor is prepared using simple, fast and cost-effective electrochemical deposition technique for detection of hydrogen peroxide. The PtNPs-SeNPs-FTO nanostructure electrodes demonstrate high electrochemical sensing activity towards H_2O_2 which is applicable in the field of clinical diagnostic, food processing, environmental analysis, pharmaceutical, and biomedical. The SeNPs-FTO, PtNPs-FTO, PtNPs-SeNPs-FTO shows a wide range of linear concentration response from 0.01 to 40 mM and response time 0.5 s. The limit of detection for PtNPs-SeNPs-FTO is 0.005 mM. The synthesized SeNPs-FTO, PtNPs-FTO and PtNPs-SeNPs-FTO sensor shows sensitivity of 0.4 μA mM^{-1} cm^{-2} ($R^2 = 0.9904$), 17.2 μA mM^{-1} cm^{-2} ($R^2 = 0.9917$), and 7.3 μA mM^{-1} cm^{-2} ($R^2 = 0.9835$) respectively. Interference investigation confirms that the capability of SeNPs-FTO, PtNPs-FTO and PtNPs-SeNPs-FTO electrodes for H_2O_2 detection through non-enzymatic electrochemical sensing which clears that PtNPs-SeNPs-FTO is highly selective towards H_2O_2. PtNPs-SeNPs-FTO nanocomposites sensor is novel, economical and shows higher selectivity as compared to PtNPs-FTO sensor.

CRediT authorship contribution statement

Mausumi Mukhopadhyay conceptualized the research work and supervised the work done all through with details contribution in discussing and reviewing of the manuscript with technical inputs. **Nilesh S. Dumore** as part of his Ph.D. research performed all the experiments, characterization, and test, calculation, drawn all figures, and data analysis of all results and wrote the manuscript.

Declaration of Competing Interest

The authors declare that they have no known competing financial interests or personal relationships that could have appeared to influence the work reported in this paper.

Acknowledgments

We are grateful to the Sophisticated Analytical Instrument Facility (SAIF), IIT Bombay, Mumbai and Materials Research Centre, MNIT Jaipur for providing the research facility for characterizations of samples. We also thankful to Ministry of Education (MoE), Government of India, India for providing fellowship and Chemical Engineering Department, SVNIT, Surat for providing research facilities.

References

[1] Y. Li, J. Zhang, J. Xuan, L. Jiang, J. Zhu, Fabrication of a novel nonenzymatic hydrogen peroxide sensor based on Se/Pt nanocomposites, Electrochem. Commun. 12 (2010) 777–780, https://doi.org/10.1016/j.elecom.2010.03.031.
[2] B. Thirumalraj, D.H. Zhao, S.M. Chen, S. Palanisamy, Non-enzymatic amperometric detection of hydrogen peroxide in human blood serum samples using a modified silver nanowire electrode, J. Colloid Interface Sci. 470 (2016) 117–122, https://doi.org/10.1016/j.jcis.2016.02.049.
[3] Y. Shu, W. Zhang, X. Yin, L. Zhang, Y. Yang, D. Ma, Q. Gao, Efficient electrochemical biosensing of hydrogen peroxide on bimetallic $Mo_{1-x}W_xS_2$ nanoflowers, J. Colloid Interface Sci. 566 (2020) 248–256, https://doi.org/10.1016/j.jcis.2020.01.083.
[4] J. Vinoth Kumar, R. Karthik, S.M. Chen, N. Raja, V. Selvam, V. Muthuraj, Evaluation of a new electrochemical sensor for selective detection of non-enzymatic hydrogen peroxide based on hierarchical nanostructures of zirconium molybdate, J. Colloid Interface Sci. 500 (2017) 44–53, https://doi.org/10.1016/j.jcis.2017.03.113.
[5] B. Halliwell, M.V. Clement, L.H. Long, Hydrogen peroxide in the human body, FEBS Lett. 486 (2000) 10–13, https://doi.org/10.1016/S0014-5793(00)02197-9.
[6] M. Braik, L.G. Zamfir, L. Rotariu, C. Curutiu, M.C. Chifiriuc, M. Ben Ali, C. Bala, An enzyme-free hydrogen peroxide sensor for evaluation of probiotic potential of

Enterococcus faecium, Sens. Actuators B Chem. 273 (2018) 298–304, https://doi.org/10.1016/j.snb.2018.06.057.
[7] J. Huang, Y. Zhu, H. Zhong, X. Yang, C. Li, Dispersed CuO nanoparticles on a silicon nanowire for improved performance of nonenzymatic H_2O_2 detection, ACS Appl. Mater. Interfaces 6 (2014) 7055–7062, https://doi.org/10.1021/am501799w.
[8] M. Liu, S. He, W. Chen, Co_3O_4 nanowires supported on 3D N-doped carbon foam as an electrochemical sensing platform for efficient H_2O_2 detection, Nanoscale 6 (2014) 11769–11776, https://doi.org/10.1039/c4nr03043e.
[9] H. Li, Y. Guo, L. Xiao, B. Chen, A fluorometric biosensor based on H_2O_2 sensitive nanoclusters for the detection of acetylcholine, Biosens. Bioelectron. 59 (2014) 289–292, https://doi.org/10.1016/j.bios.2014.03.054.
[10] U. Pinkernell, S. Effkemann, U. Karst, Simultaneous HPLC determination of peroxyacetic acid and hydrogen peroxide, Anal. Chem. 69 (1997) 3623–3627, https://doi.org/10.1021/ac9701750.
[11] J.E. Frew, P. Jones, G. Scholes, Spectrophotometric determination of hydrogen peroxide and organic hydroperoxides at low concentrations in aqueous solution, Anal. Chim. Acta 16 (1987) 215–230.
[12] L. Luo, Z. Zhang, Sensors based on galvanic cell generated electrochemiluminescence and its application, Anal. Chim. Acta 580 (2006) 14–17, https://doi.org/10.1016/j.aca.2006.07.039.
[13] Z. Rosenzweig, R. Kopelman, Analytical properties and sensor size effects of a micrometer-sized optical fiber glucose biosensor, Anal. Chem. 68 (1996) 1408–1413, https://doi.org/10.1021/ac950864g.
[14] P. Chakraborty, S. Dhar, K. Debnath, S.P. Mondal, Glucose and hydrogen peroxide dual-mode electrochemical sensing using hydrothermally grown CuO nanorods, J. Electroanal. Chem. 833 (2019) 213–220, https://doi.org/10.1016/j.jelechem.2018.11.060.
[15] E. Formo, Z. Peng, E. Lee, X. Lu, H. Yang, Y. Xia, Direct oxidation of methanol on Pt nanostructures supported on electrospun nanofibers of anatase, J. Phys. Chem. C 112 (2008) 9970–9975, https://doi.org/10.1021/jp803763q.
[16] F. Jia, C. Yu, K. Deng, L. Zhang, Nanoporous metal (Cu, Ag, Au) films with high surface area: general fabrication and preliminary electrochemical performance, J. Phys. Chem. C 111 (2007) 8424–8431, https://doi.org/10.1021/jp071815y.
[17] C. Xu, Y. Liu, F. Su, A. Liu, H. Qiu, Nanoporous PtAg and PtCu alloys with hollow ligaments for enhanced electrocatalysis and glucose biosensing, Biosens. Bioelectron. 27 (2011) 160–166, https://doi.org/10.1016/j.bios.2011.06.036.
[18] N.S.K. Gowthaman, S.A. John, M. Tominaga, Fast growth of Au-Pt bimetallic nanoparticles on SWCNTs: composition dependent electrocatalytic activity towards glucose and hydrogen peroxide, J. Electroanal. Chem. 798 (2017) 24–33, https://doi.org/10.1016/j.jelechem.2017.05.029.
[19] H. Lu, S. Yu, Y. Fan, C. Yang, D. Xu, Nonenzymatic hydrogen peroxide electrochemical sensor based on carbon-coated SnO_2 supported Pt nanoparticles, Colloids Surf. B Biointerfaces 101 (2013) 106–110, https://doi.org/10.1016/j.colsurfb.2012.05.033.
[20] H. Wang, X. Bo, J. Bai, L. Wang, L. Guo, Electrochemical applications of platinum-palladium alloy nanoparticles/large mesoporous carbon, J. Electroanal. Chem. 662 (2011) 281–287, https://doi.org/10.1016/j.jelechem.2011.06.020.
[21] J.M. You, D. Kim, S. Jeon, Electrocatalytic reduction of H_2O_2 by Pt nanoparticles covalently bonded to thiolated carbon nanostructures, Electrochim. Acta 65 (2012) 288–293, https://doi.org/10.1016/j.electacta.2012.01.070.
[22] P.X. Gao, C.S. Lao, Y. Ding, Z.L. Wang, Metal/semiconductor core/shell nanodisks and nanotubes, Adv. Funct. Mater. 16 (2006) 53–62, https://doi.org/10.1002/adfm.200500301.
[23] M.K. Lee, T.G. Kim, W. Kim, Y.M. Sung, Surface plasmon resonance (SPR) electron and energy transfer in noble metal-zinc oxide composite nanocrystals, J. Phys. Chem. C 112 (2008) 10079–10082, https://doi.org/10.1021/jp8018809.
[24] N.S. Dumore, M. Mukhopadhyay, Antioxidant properties of aqueous selenium nanoparticles (ASeNPs) and its catalysts activity for 1, 1-diphenyl-2-picrylhydrazyl (DPPH) reduction, J. Mol. Struct. 1205 (2020), 127637.
[25] H. Zhang, D. Yang, Y. Ji, X. Ma, J. Xu, D. Que, Selenium nanotubes synthesized by a novel solution phase approach, J. Phys. Chem. B 108 (2004) 1179–1182, https://doi.org/10.1021/jp036168z.
[26] B. Mayers, X. Jiang, D. Sunderland, B. Cattle, Y. Xia, Hollow nanostructures of platinum with controllable dimensions can be synthesized by templating against selenium nanowires and colloids, J. Am. Chem. Soc. 125 (2003) 13364–13365, https://doi.org/10.1021/ja0379722.
[27] K.S. Prasad, J.V. Vaghasiya, S.S. Soni, J. Patel, R. Patel, M. Kumari, F. Jasmani, Microbial selenium nanoparticles (SeNPs) and their application as a sensitive hydrogen peroxide biosensor, Appl. Biochem. Biotechnol. 177 (2015) 1386–1393, https://doi.org/10.1007/s12010-015-1814-9.
[28] J. Zhang, S.Y. Zhang, J.J. Xu, H.Y. Chen, A new method for the synthesis of selenium nanoparticles and the application to construction of H_2O_2 biosensor, Chinese Chem. Lett. 15 (2004) 1345–1348. ⟨http://www.imm.ac.cn/journal/ccl.html⟩.
[29] F. Lamberti, S. Agnoli, L. Brigo, G. Granozzi, M. Giomo, N. Elvassore, Surface functionalization of fluorine-doped tin oxide samples through electrochemical grafting, Appl. Mater. Interfaces 5 (2013) 12887–12894, https://doi.org/10.1021/am403292x.
[30] E. Scavetta, B. Ballarin, M. Gazzano, D. Tonelli, Electrochemical behaviour of thin films of Co/Al layered double hydroxide prepared by electrodeposition, Electrochim. Acta 54 (2009) 1027–1033, https://doi.org/10.1016/j.electacta.2008.07.078.
[31] O. Dilmi, M. Benaicha, Electrodeposition and characterization of red selenium thin film-effect of the substrate on the nucleation mechanism, Russ. J. Electrochem. 53 (2017) 140–146, https://doi.org/10.1134/S1023193517020045.
[32] E. Scavetta, A. Casagrande, I. Gualandi, D. Tonelli, Analytical performances of Ni LDH films electrochemically deposited on Pt surfaces: phenol and glucose detection, J. Electroanal. Chem. 722–723 (2014) 15–22, https://doi.org/10.1016/j.jelechem.2014.03.018.
[33] S. Shahrokhian, S. Rastgar, Construction of an electrochemical sensor based on the electrodeposition of Au-Pt nanoparticles mixtures on multi-walled carbon nanotubes film for voltammetric determination of cefotaxime, Analyst 137 (2012) 2706–2715, https://doi.org/10.1039/c2an35182j.
[34] H. Liu, A. Wang, Q. Sun, T. Wang, H. Zeng, Cu nanoparticles/fluorine-doped tin oxide (FTO) nanocomposites for photocatalytic H_2 evolution under visible light irradiation, Catalysts 7 (2017), https://doi.org/10.3390/catal7120385.
[35] J. Zhang, J. Han, Z. Shi, Y. Ju, Z. Zhang, M. Gu, Fabrication and enhanced H_2O_2 sensing properties of the uniform porous FTO glasses with tunable pore sizes and densities, Appl. Surf. Sci. 465 (2019) 357–361.
[36] A.A. Aal, F. Voigts, D. Chakarov, F. Endres, Electrodeposition of selenium from 1-butyl-1-methylpyrrolidinium trifluoromethylsulfonate, Electrochim. Acta 59 (2012) 228–236, https://doi.org/10.1016/j.electacta.2011.10.064.
[37] N.S. Dumore, M. Mukhopadhyay, Sensitivity enhanced SeNPs-FTO electrochemical sensor for hydrogen peroxide detection, J. Electroanal. Chem. 878 (2020), 114544, https://doi.org/10.1016/j.jelechem.2020.114544.
[38] X. Chang, C. Batchelor-McAuley, R.G. Compton, Hydrogen peroxide reduction on single platinum nanoparticles, Chem. Sci. 11 (2020) 4416–4421, https://doi.org/10.1039/d0sc00379d.
[39] R. Abdel-Karim, Y. Reda, A. Abdel-Fattah, Review-nanostructured materials-based nanosensors, J. Electrochem. Soc. 167 (2020), 037554, https://doi.org/10.1149/1945-7111/ab67aa.
[40] D. Thatikayala, D. Ponnamma, K.K. Sadasivuni, J. Cabibihan, A.K. Al-ali, R. A. Malik, B. Min, Progress of advanced nanomaterials in the non-enzymatic electrochemical sensing of glucose, Biosensors 10 (2020) 151.
[41] T. Wang, L. Yang, B. Zhang, J. Liu, Extracellular biosynthesis and transformation of selenium nanoparticles and application in H_2O_2 biosensor, Colloids Surf. B Biointerfaces 80 (2010) 94–102, https://doi.org/10.1016/j.colsurfb.2010.05.041.
[42] G. Yu, W. Wu, X. Pan, Q. Zhao, X. Wei, Q. Lu, High sensitive and selective sensing of hydrogen peroxide released from pheochromocytoma cells based on Pt-Au bimetallic nanoparticles electrodeposited on reduced graphene sheets, Sensors 15 (2015) 2709–2722, https://doi.org/10.3390/s150202709.
[43] Y. Zhang, X. Wang, Y. Zhu, H. Jiang, X. Bai, K.-K. Shiu, Highly sensitive graphene-Pt nanocomposites amperometric biosensor and its application in living cell H_2O_2 detection, Anal. Chem. 86 (2014) 9459–9465, https://doi.org/10.1021/ac5009699.
[44] D. Lu, Y. Zhang, S. Lin, L. Wang, C. Wang, Synthesis of PtAu bimetallic nanoparticles on graphene–carbon nanotube hybrid nanomaterials for nonenzymatic hydrogen peroxide sensor, Talanta 112 (2013) 111–116, https://doi.org/10.1016/j.talanta.2013.03.010.